Use of a Mouse In Vitro Fertilization Model to Understand the Developmental Origins of Health and Disease Hypothesis

Sky K. Feuer,* Xiaowei Liu,* Annemarie Donjacour, Wingka Lin, Rhodel K. Simbulan, Gnanaratnam Giritharan, Luisa Delle Piane, Kevin Kolahi, Kurosh Ameri, Emin Maltepe, and Paolo F. Rinaudo

Department of Obstetrics, Gynecology and Reproductive Sciences (S.K.F., X.L., A.D., W.L., R.K.S., G.G., L.D.P., K.K., P.F.R.), and Department of Pediatrics (K.A., E.M.), University of California San Francisco, San Francisco, California 94143; Nevada Center for Reproductive Medicine (G.G.), Reno, Nevada 89511; Obstetric and Gynecology Department (L.D.P.), University of Turin, Turin, Italy; and Oregon Health & Science University (K.K.), Portland, Oregon 97239

The Developmental Origins of Health and Disease hypothesis holds that alterations to homeostasis during critical periods of development can predispose individuals to adult-onset chronic diseases such as diabetes and metabolic syndrome. It remains controversial whether preimplantation embryo manipulation, clinically used to treat patients with infertility, disturbs homeostasis and affects long-term growth and metabolism. To address this controversy, we have assessed the effects of in vitro fertilization (IVF) on postnatal physiology in mice. We demonstrate that IVF and embryo culture, even under conditions considered optimal for mouse embryo culture, alter postnatal growth trajectory, fat accumulation, and glucose metabolism in adult mice. Unbiased metabolic profiling in serum and microarray analysis of pancreatic islets and insulin sensitive tissues (liver, skeletal muscle, and adipose tissue) revealed broad changes in metabolic homeostasis, characterized by systemic oxidative stress and mitochondrial dysfunction. Adopting a candidate approach, we identify thioredoxin-interacting protein (TXNIP), a key molecule involved in integrating cellular nutritional and oxidative states with metabolic response, as a marker for preimplantation stress and demonstrate tissue-specific epigenetic and transcriptional TXNIP misregulation in selected adult tissues. Importantly, dysregulation of TXNIP expression is associated with enrichment for H4 acetylation at the *Txnip* promoter that persists from the blastocyst stage through adulthood in adipose tissue. Our data support the vulnerability of preimplantation embryos to environmental disturbance and demonstrate that conception by IVF can reprogram metabolic homeostasis through metabolic, transcriptional, and epigenetic mechanisms with lasting effects for adult growth and fitness. This study has wide clinical relevance and underscores the importance of continued follow-up of IVF-conceived offspring. **(*Endocrinology* 155: 1956–1969, 2014)**

The Developmental Origins of Health and Disease (DOHaD) hypothesis postulates that during critical periods in development, organisms exhibit a developmental plasticity that enables them to fine-tune patterns of gene expression in accordance with environmental cues. Such changes often confer immediate survival advantages; however, transient stresses experienced in utero may also induce inappropriate adaptive changes that conflict with postnatal environments and impair adult health (1). More recently, it has been demonstrated that fertilization and preimplantation development are periods of environmental vulnerability (2, 3).

Preimplantation development is characterized by highly coordinated physiological and epigenetic changes

ISSN Print 0013-7227 ISSN Online 1945-7170
Printed in U.S.A.

Received November 22, 2013. Accepted March 18, 2014.
First Published Online January 31, 2014

* S.K.F. and X.L. contributed equally to this work.

Abbreviations: ART, assisted reproductive technology; FB, flushed blastocyst; H4ac, acetylated H4; IPGTT, ip glucose tolerance test; IVF, in vitro fertilization; KAA, KSOM supplemented with amino acids; KSOM, potassium simple optimized medium; SDS, sodium dodecyl sulfate; TXNIP, thioredoxin-interacting protein; WM, Whitten's medium.

as the zygote develops to blastocyst. The diverse energy requirements supporting this transition are satisfied by the differential availability of nutrients, oxygen, and growth signals as the embryo travels from the oviduct to uterus (4). Importantly, this dynamic metabolic environment is lost with embryo culture in vitro (reviewed in Reference 5).

Manipulation of preimplantation embryos by means of assisted reproductive technologies (ART), such as in vitro fertilization (IVF), is widely used for breeding livestock and to treat infertility in humans. In fact, ART has contributed to the successful birth of more than 5 million individuals worldwide, and now accounts for approximately 60 000 births annually in the United States (6). Although the majority of IVF children appear healthy, the slightly increased prevalence of birth malformations, cancer, and imprinting disorders indicates possible dangers associated with ART (reviewed in Reference 7). More recently, reports of metabolic and cardiovascular irregularities in IVF adolescents, including modest increases in blood pressure, fasting glucose, fat deposition, and growth velocity, may signify a lasting effect of IVF on postnatal growth and metabolic health (8, 9), although this issue remains controversial (10). Because IVF offspring are at most 35 years of age, the effects of this procedure on the later stages of development and adult disease susceptibility are uncertain.

The current study addresses the impact of IVF on postnatal growth and adult metabolic health in mice. To evaluate whether different culture conditions have different long-term effects, we selected both a stressful (Whitten's medium, IVF_{WM}), and optimized medium (potassium simple optimized medium [KSOM], supplemented with amino acids [IVF_{KAA}]) for evaluation (Supplemental Figure 1) (11). Initial discovery experiments were performed culturing embryos in an environment with high oxygen concentration (20% O_2) and WM, a medium characterized by high glucose concentration (5.5 mM) and the lack of glutamine and amino acids, to evaluate whether abnormalities in growth were present (3). Having identified an effect, we performed a large series of experiments using the more clinically relevant KSOM associated with physiologic oxygen concentration (5% O_2) (13). As a control, C57Bl/6J females were superovulated and mated overnight with C57Bl/6J males, and the in vivo-generated blastocysts were isolated 96 hours postfertilization for use directly in experiments or transfer to recipients (flushed blastocyst [FB] group), as we have previously reported (14, 15). The FB group is a more suitable control than simply using females postmating, because it accounts for superovulation, litter size, and the embryo transfer procedure. Indeed the embryo transfer procedure alone has been shown to alter expression of imprinted genes (16).

We provide evidence that preimplantation disturbance can alter postnatal growth trajectory and impair adult glucose and lipid metabolism in a sex-, tissue-, and culture condition-specific fashion. This indicates that individual stresses experienced transiently during development may have unique and lasting consequences for adult metabolism. Further, we identify up-regulation of thioredoxin-interacting protein (TXNIP, also known as VDUP-1, TBP-2) as a candidate marker of preimplantation disturbance. TXNIP is the principal inhibitor of thioredoxin, a key cellular antioxidant, and elevated levels of TXNIP are associated with impaired glucose tolerance (17), oxidative stress (18), and apoptosis (19). Txnip is subject to epigenetic regulation under conditions of metabolic stress (20), and we demonstrate sustained epigenetic alteration to the *Txnip* locus, providing mechanistic insight into the DOHaD hypothesis with regard to stress-induced reprogramming of embryo metabolism.

Materials and Methods

For detailed description see Supplemental *Materials and Methods*.

Animals, IVF, embryo culture, and transfer

All animals were maintained according to institutional regulations, under a constant 12 hour light/dark cycle with ad libitum access to water and chow (PicoLab; 5058). To probe the consequences of nutritional stress the FB and IVF_{KAA} cohorts were exposed to a high-fat diet beginning at 24 weeks of age (Research Diets, Inc; D12494). IVF, embryo culture, and embryo transfer experiments were performed as previously described (21). Briefly, C57BL/6J virgin females 6–8 weeks of age (~20–23 g) were injected with 5 IU pregnant mare serum gonadotropin followed 46–48 hours later by 5 IU human chorionic gonadotropin to induce superovulation. Cumulous-oocyte-complexes were isolated from ampullae 13–15 hours after human chorionic gonadotropin administration and incubated 4–6 hours in HTF medium (Millipore Corp; MR-070-D) with sperm obtained from capacitated (1 hour) cauda epididymal sperm of C57BL/6J males. Fertilized zygotes were washed and cultured to the blastocyst stage at 37°C under Ovoil (Vitrolife; 10029). Zygotes were cultured using either: 1) Whitten's medium (WM) under 20% oxygen (ie, suboptimal culture conditions), or 2) potassium simplex optimization medium with amino acids (KAA; Millipore, MR-106-D) under 5% oxygen in a modular humidified chamber. Embryos were transferred to pseudopregnant CF-1 recipient females. Therefore, 3 groups were generated: 1) The IVF_{WM} group (n = 9 litters;) cultured in stressful conditions; 2) The IVF_{KAA} cohort (n = 11 litters) cultured in optimal conditions; 3) The FB controls (n = 18 litters) were generated at 2 time points. To rule out possible litter size effects (22), among the litters generated, we chose only to maintain litters consisting of 4–8 animals in IVF_{KAA} (5 litters of size: 4, 5, 5, 5, and 7) and its comparison FB (3 litters of size 5, 6, and8) and 3–6 animals in the IVF_{WM} (5 litters of size 3, 3, 4, 5, and 6) and its FB com-

parison (4 litters of size 3, 3, 4, 5). We found no differences in growth or glucose handling when comparing animals deriving from small (n = 3–4 pups or less) or large (n = 5–8) litters.

Body weight, morphometrics, food intake, and body composition analyses

Animals were weighed weekly beginning at birth. Food intake was measured daily for 1 week at ages 7, 20, and 28 weeks. Fat and lean body mass, percent fat, whole-body areal bone mineral density, and bone mineral content were determined at 8, 16, 21, and 29 weeks of age by dual-energy X-ray absorptiometry, using a Lunar PIXImus II mouse densitometer.

Histology

Dissected kidneys were fixed in 4% paraformaldehyde, bisected through the ureter, and paraffin-embedded for coronal sectioning. Glomerular density was estimated using the dissector method (23). β-Cell mass was quantified using an unbiased fractionator sampling scheme to compensate for possible heterogeneous islet distribution within the pancreas (24).

Glucose tolerance and plasma measurements

Glucose tolerance was assessed at approximately 19 and 35 weeks (for IVF_{WM}) and 8, 20, and 29 weeks (IVF_{KAA}) of age. IVF_{WM} mice were fasted overnight (25). IVF_{KAA} were fasted for 6 hours, because this protocol was found to be more sensitive to detect abnormalities in glucose handling (26). After fasting with ad libitum access to water, baseline glucose values were individually established using a handheld glucometer, and 50-μL blood samples were collected from tail tips for plasma composition analyses. Clearance of a 1.5 mg/g glucose bolus injected ip was subsequently monitored at 15, 30, 60, and 120-minute intervals after injection. Plasma levels of insulin and leptin were quantified using a mouse serum adipokine LINCOplex kit (Millipore; MADPK-71K), as directed by the manufacturer. Plasma cortisol was determined via the GammaCoat Cortisol [^{125}I]RIA kit (Diasorin; CA1529), as previously described (27).

Islet isolation and in vitro insulin secretion assay

Islets of Langerhans were isolated from surrounding exocrine pancreas in mice aged 29 weeks by the University of California San Francisco Islet Production Core Facility according to standard procedures (28).

Microarray preparation and analysis

Microarray experiments were conducted as we have previously reported (29), using 4 tissues (liver, gastrocnemius muscle, gonadal fat, pancreatic islets) derived from 3 adult FB and IVF_{KAA} female mice (24 independent microarrays). Animals contributing to this analysis were derived from at least 2 separate litters of 5–7 pups per condition, and to minimize variation, each animal provided the 4 tissues. Total RNA was extracted, purified, and hybridized to Affymetrix Mouse Gene 1.0 ST arrays.

Metabolomic profiling

Unbiased metabolomic profiling of serum (n = 4 IVF_{KAA} and 4 FB females) was performed by Metabolon, Inc, as described in detail elsewhere (30).

Antibodies

The following primary antibodies were used in this study: rabbit pAb to Oct3/4 (Santa Cruz Biotechnology; sc-9081), mouse mAb to VDUP-1/Txnip (MBL; k0204–3), rabbit pAb to Txnip (Abcam; ab86983), mouse mAb to α-tubulin (Sigma; T9026), rabbit pAb to Actin (Sigma; A2103), rabbit pAb to acetyl-H4 (Millipore; 06–866), rabbit pAb to H4K20me3 (Diagenode; pAb-057–050), normal rabbit IgG (Millipore; 12–370). Secondary antibodies included IRDye 800CW goat antirabbit and IRDye 680 goat antimouse (LI-COR). Secondary antibodies used for immunofluorescence were AlexaFluor 594 goat antirabbit IgG (Invitrogen; A11012) and AlexaFluor 488 chicken antimouse IgG (Invitrogen; A21200).

Immunofluorescence

Blastocysts were fixed 15 minutes in ice-cold methanol at −20°C, washed with PBS, and blocked 1 hour in PBS containing 5% BSA and 0.5% Tween 20. Cells were incubated overnight at 4°C with primary antibody diluted in PBS and 5% BSA, washed, and incubated 1 hour at 4°C with secondary antibody diluted in blocking solution. After a final wash, blastocysts were mounted with 4′,6-diamidino-2-phenylindole-containing mounting solution (Vectashield; H-1200) and visualized at the UCSF Biological Imaging Development Center with a Zeiss Imager Z.2 fluorescent microscope equipped with an Apotome and Axiovision software for optical sectioning and analyzing.

Chromatin immunoprecipitation

A previously optimized micro chromatin immunoprecipitation protocol using as little as 50 mg fat tissue or 100 pooled blastocysts (~10 000 cells) was conducted as described elsewhere (31), with minor modification.

Quantitative real-time PCR

Blastocysts developed in vivo or in vitro (WM with 20% oxygen or KAA with 5% oxygen) were collected as described above, and quantitative real-time PCR was conducted on 5 independent biological replicates containing 5 or more pooled blastocysts (29).

Immunoblotting

Extracts for SDS-PAGE were prepared either from pools of 10 blastocysts lysed in cold urea lysis buffer (8 M urea, 10% glycerol, 5 mM dithiothreitol, 10 mM Tris-HCl, pH 6.8, 1% sodium dodecyl sulfate [SDS], with protease inhibitors), or whole fat or muscle tissues homogenized in cold tissue extraction buffer (100 mM Tris, 2 mM Na_3VO_4, 100 mM NaCI, 1% Triton X-100, 1 mM EDTA, 10% glycerol, 1% EGTA, 0.1% SDS, 1 mM NaF, 0.5% deoxycholate, 20% $Na_4P_2O_7$, with protease inhibitors). Protein levels were quantified by BCA protein assay (Thermo Scientific). Tissue (15 μg) or 10 blastocysts-equivalent lysates were subjected to gel electrophoresis on 12% PAGEr Gold Precast gels (Lonza) and blotted on to Immobilon-FL membranes (Millipore) using semidry transfer (Bio-Rad Laboratories). Dried membranes were reactivated in methanol, rinsed with PBS, and blocked in Odyssey Blocking Buffer (LI-COR Biosciences; 927–40000). Membranes were then probed overnight at 4°C with primary antibodies diluted 1:1000 in blocking buffer with 0.1% Tween 20, washed in PBS, and incubated with secondary antibody diluted in blocking buffer containing 0.1% SDS and 0.1%

Tween 20. Protein signal detection was performed using the LI-COR Odyssey Imaging System.

DNA methylation analysis

Genomic DNA was extracted from pools of 10 blastocysts by standard proteinase K digestion containing SDS and yeast tRNA, and processed using the MethylEasy Xceed rapid sodium bisulfite modification kit (Takara) according to manufacturer's instructions.

Statistics

All data are presented as the mean ± SD, unless otherwise specified. Either a one-way ANOVA or a two-tailed Student's *t* test was used for statistical analysis, as appropriate. Tukey's post hoc correction was applied to test for differences between groups when a one-way ANOVA was significant.

Results

IVF under suboptimal conditions affects growth and glucose homeostasis

Conception using suboptimal conditions (ie, IVF_{WM}) impaired postnatal growth by 2 weeks of age. Both IVF_{WM} males and females were significantly smaller in size compared with FB controls (Figure 1, A and C) and remained smaller throughout the postnatal period until time of death at 35–40 weeks. IVF_{WM} did not affect litter size, birth weight, anogenital distance, crown-rump length, body mass index, or head or abdominal diameter (Supplemental Figure 2). Anogenital index (anogenital distance standardized to body weight), a measure of prenatal androgen exposure (32), was however significantly larger in male IVF_{WM} animals. These birth data indicate that external physiology of IVF concepti at birth is not a reliable indicator of postnatal growth or adult glucose homeostasis.

Because decreased neonatal growth is linked to impaired glucose homeostasis and the development of type 2 diabetes (33), we examined glucose metabolism by ip glucose tolerance tests (IPGTT) at 19 weeks of age. Blood glucose levels following glucose administration were significantly higher in IVF_{WM} female mice ($P < .05$; Figure 1, B and D), with a trend toward significance in males ($P = .06$).

To evaluate the long-term impacts of IVF on metabolic homeostasis, blood samples were collected from fed and 4-hour fasted animals at 35 weeks for plasma insulin, leptin, and corticosterone determination. Insulin levels were not statistically different, but systemic leptin was greater in IVF_{WM} females in the fed state compared with controls (Supplemental Figure 2, A and B). Corticosterone levels were not different in fed or fasting conditions between the 2 conception groups. However, IVF_{WM} males did not show the expected increase in corticosterone levels fol-

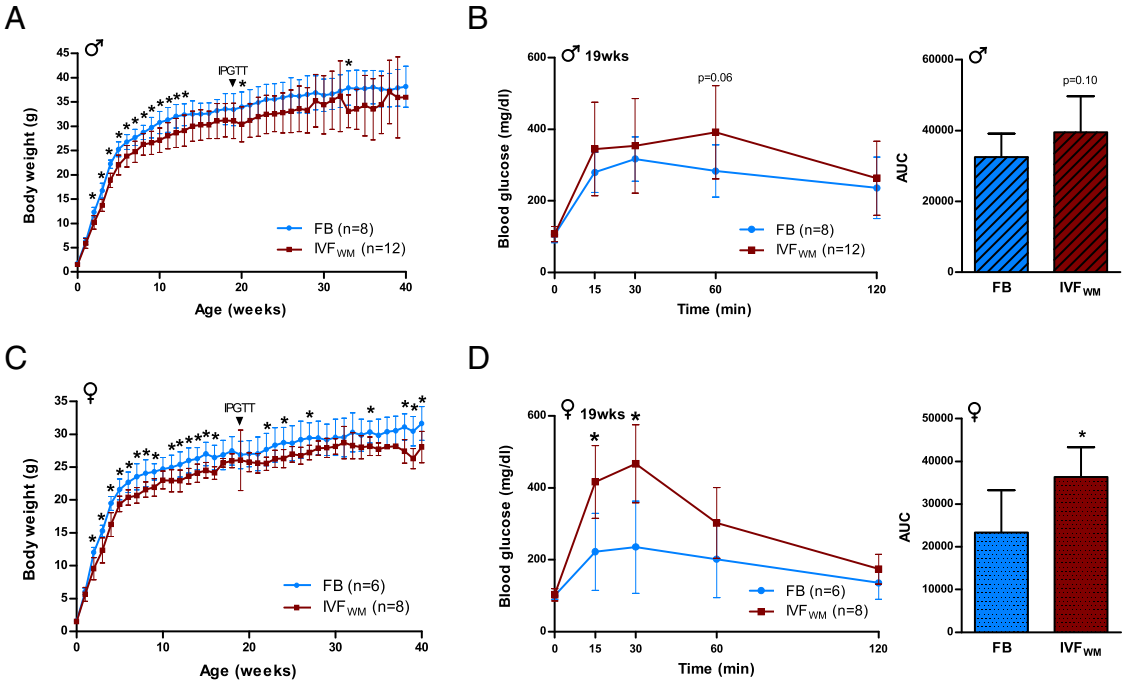

Figure 1. Conception by IVF_{WM} reduces growth and impairs glucose tolerance. A, Postnatal growth curves depicting average body weight for male FB (blue) and IVF_{WM} (red) mice. B, Male IPGTT sampled at 19 weeks for clearance of a 1.5 mg/g glucose bolus over 120 minutes, with area under the curve (AUC) calculated from total glucose levels measured during the entire IPGTT course. C, Postnatal growth of female FB and IVF_{WM} animals, and (D) female IPGTT sampled in tandem with males. For all measurements: FB males, n = 8; IVF_{WM} males, n = 12; FB females, n = 6; IVF_{WM} females, n = 8. Error bars depict SD. *, $P < .05$.

lowing fasting as observed in control mice, suggesting a blunted response to nutritional stress.

At time of death (35–40 weeks), body mass index and anogenital distance were lower in both IVF_{WM} males and females, and female IVF_{WM} mice weighed significantly less than controls (Supplemental Figure 2, C–E). Interestingly, thymus weight was greater after weight standardization in IVF_{WM} animals (significant in males, a trend toward significance in females; Supplemental Figure 2, F and G). There was markedly less global fat in IVF_{WM} females at 40 weeks, whereas males displayed lower mesenteric adipose weight only. We conducted histologic analyses of renal and pancreas tissue to assess for evidence of end-organ damage but detected no changes in glomerular number or volume or percent of pancreatic tissue staining positively for insulin (Supplemental Figure 3).

IVF under optimal conditions alters fat composition and insulin secretion in females

The initial observation that IVF and embryo culture under stressful conditions perturbs adult metabolism led us to design additional and more extensive experiments using optimized conditions, because WM does not accurately reproduce current IVF clinical practices. We selected KSOM containing amino acids, considered optimal for mouse embryo culture (34), with 5% oxygen levels (IVF_{KAA}). Importantly, many IVF clinics use media derived from KSOM, making its use clinically relevant. IVF_{KAA} mice were used for all subsequent analyses reported in this study. As with the IVF_{WM} group, only litters of 4–8 animals were maintained to remove potential confounding effects of litter size.

Females

From birth, we observed a marked sexually dimorphic effect of IVF_{KAA}. Female IVF_{KAA} pups exhibited significantly lower birth weight, anogenital distance, crown-rump length, and head diameter at birth (Supplemental Table 1). After birth, birth weights were similar between the 2 cohorts until 17 weeks of age, at which point IVF_{KAA} females became heavier than controls (Figure 2A). Because latent growth alterations have been associated with metabolic disease (35), we probed the consequences of nutritional stress by challenging both cohorts with a high-fat diet beginning at 24 weeks. All animals displayed comparable changes in weight. IVF_{KAA} females consumed more food at 7 and 20 weeks of age, but average intake at 28 weeks, after placement on the high-fat diet, equaled control amounts (Figure 2B). Dual-energy X-ray absorptiometry scanning at 8, 16, 21, and 28 weeks revealed increased bone mineral density in IVF_{KAA} females at 8, 21, and 28 weeks of age (Figure 2D). We additionally observed continuous accumulation of fat throughout postnatal life: body fat percentage was initially lower in IVF_{KAA} than FB females, but the IVF_{KAA} animals steadily accrued fat mass and surpassed control levels by 21 weeks of age (Figure 2, E and F). Interestingly, this increase in fat deposition occurred prior to the nutritional challenge posed by the high-fat diet.

Analysis of glucose metabolism by IPGTT at 13, 20, and 29 weeks showed no changes in glucose handling between IVF and control animals, although fasting glucose levels were significantly higher in IVF_{KAA} animals at 20 and 29 weeks (Figure 2C and Supplemental Figure 4). At 29 weeks, pancreatic islets were isolated for glucose-stimulated insulin secretion assays from IVF_{KAA} and FB females. The insulin secretory response to glucose was normal in FB animals, despite 5 weeks on the high-fat diet (Figure 2G). The effect of glucose on islet insulin secretion in IVF_{KAA} females was ablated at 29 weeks, indicating that these females are susceptible to β-cell dysfunction following nutritional stress (Figure 2H). At time of death (30 weeks), the IVF_{KAA} females were moderately heavier than controls ($P = .08$) and displayed shorter anogenital distance and smaller relative pancreatic weight (Supplemental Figure 5).

Males

For all parameters examined, male IVF_{KAA} animals were statistically indistinguishable from FB controls but displayed a trend toward significance for increased plasma insulin at 11 weeks ($P = .07$), decreased fasting glucose at 13 weeks ($P = .06$), and decreased adrenal weight at time of death ($P = .06$; Supplemental Figures 5 and 6).

Evidence of metabolic stress in IVF_{KAA} female serum metabolome

To further characterize the metabolic consequences of IVF_{KAA} in females, we performed unbiased global metabolomic profiling of IVF_{KAA} and FB serum using liquid chromatography/mass spectroscopy and gas chromatography/mass spectroscopy (Metabolon, Inc). This analysis detected 280 distinct metabolites in the plasma samples (Figure 3A), of which 35 were significantly altered in IVF_{KAA} sera (Figure 3, B and C; $P < .05$; 9 metabolites increased and 26 decreased), and 21 approached significance ($0.05 < P < .1$; 9 increased and 12 decreased). Supplemental Table 2 provides a comprehensive list of all serum biochemicals identified by the analysis. Overall, metabolite signatures in IVF_{KAA} animals reflected widespread shifts in energy metabolism. IVF_{KAA} females were clearly distinguishable from FB controls through a dramatic reduction in serum glycerophosphocholines, short-chain acyl-carnitines, and acyl-glycines. Branched amino

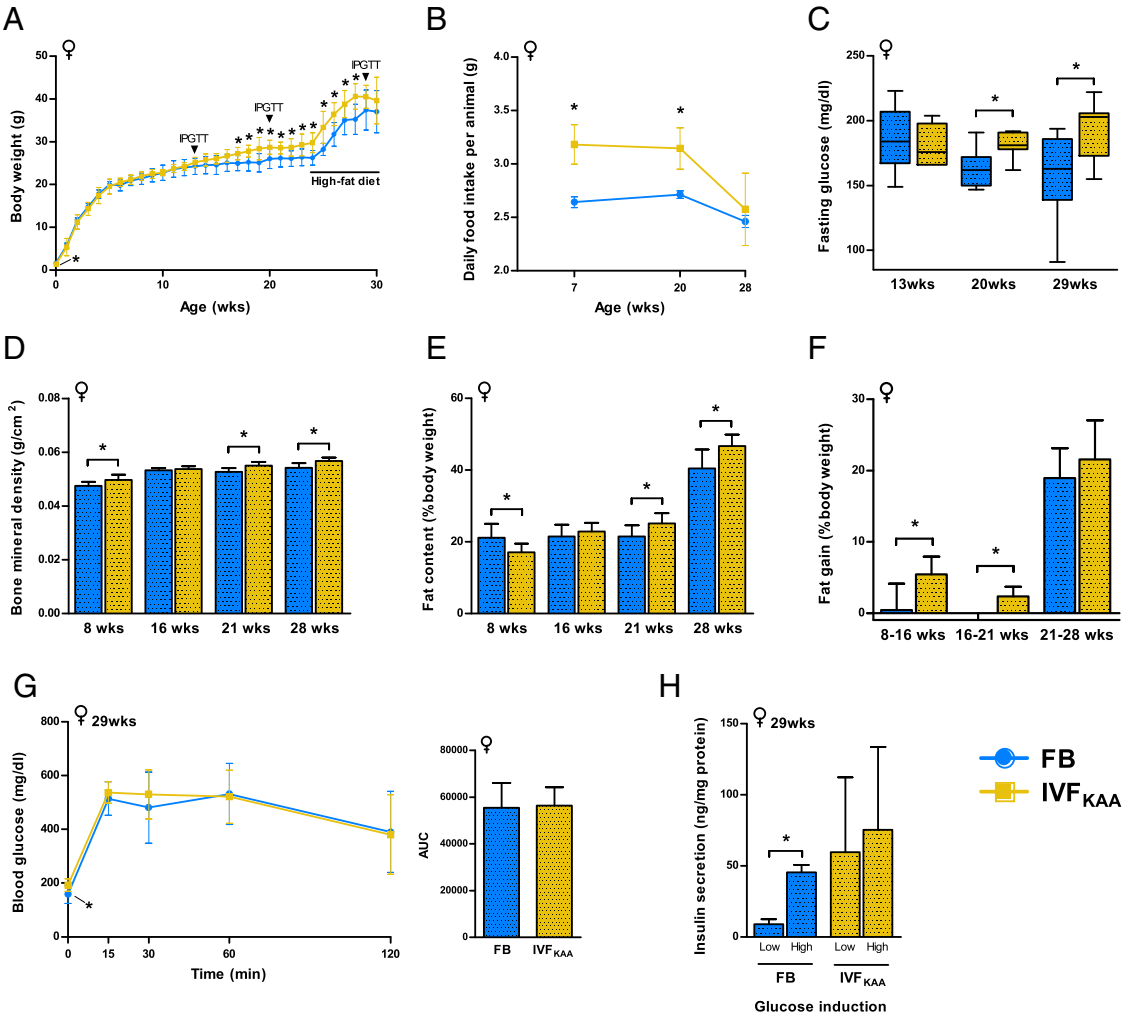

Figure 2. Evidence of glucose intolerance and altered fat deposition in IVF_{KAA} females. A, Postnatal growth of FB (blue) and IVF_{KAA} (yellow) females, showing periodic sampling of IPGTT and the administration of a high-fat diet beginning at 24 weeks. B, Average daily food intake monitored over selected 5-day periods throughout postnatal development. C, Fasting glucose levels measured during IPGTTs. D–F, Periodic dual-energy X-ray absorptiometry (DEXA) scanning of (D) bone mineral density and (E) fat content, with calculated (F) percent fat gain in FB and IVF_{KAA} females. G, IPGTT of glucose handling at 29 weeks of age, with corresponding AUC measured from total glucose levels during entire IPGTT course. H, Insulin secretion assay conducted on isolated pancreatic islets from 29-week-old FB (n = 3) and IVF_{KAA} (n = 5) females, depicting normalized insulin secretion in response to basal and stimulatory glucose challenges. For all analyses: FB, n = 8, and IVF_{KAA}, n = 7–9 females, unless indicated otherwise. Error bars depict SD. *, $P < .05$.

acid oxidation was restricted, as evidenced by the elevation of 3-methyl-2-oxobutyrate, 3-methyl-2-oxovalerate, and 4-methyl-2-oxopentanoate, in conjunction with a decrease in their derivatives isobutyrylglycine and β-hydroxyisovalerate. Additional noteworthy differences included changes in glycolytic and trichloroacetic acid (TCA) cycle intermediates, increased levels of the ketone 3-hydroxybutyrate, and depleted systemic glutamine and glutamate. Higher corticosterone levels in IVF_{KAA} bordered statistical significance ($P = .06$).

IVF_{KAA} metabolic defects are reflected in global gene expression signatures

To elucidate the molecular mechanisms underlying the impaired IVF_{KAA} energy metabolism, we used Affymetrix Mouse Gene 1.0 ST microarrays to probe gene expression profiles in pancreatic islets and insulin-sensitive tissues (liver, skeletal muscle, gonadal fat) isolated from 3 IVF_{KAA} and 3 FB female animals aged 29 weeks (Figure 4 and Supplemental Table 3). This analysis identified 1657 liver transcripts (1355 unique genes), 2724 muscle transcripts (2148 genes), 678 fat transcripts (588 genes), and 906 islet transcripts (756 genes) differentially expressed ($P < .05$) between the 2 conception conditions (Figure 4A). Processing of gene lists by Ingenuity Pathway Analysis identified multiple glucose, lipid, and transcriptional regulatory pathways in all 4 tissues that might contribute to the metabolic defects associated with IVF_{KAA}, indicating that patterns of gene expression were consistent with our physi-

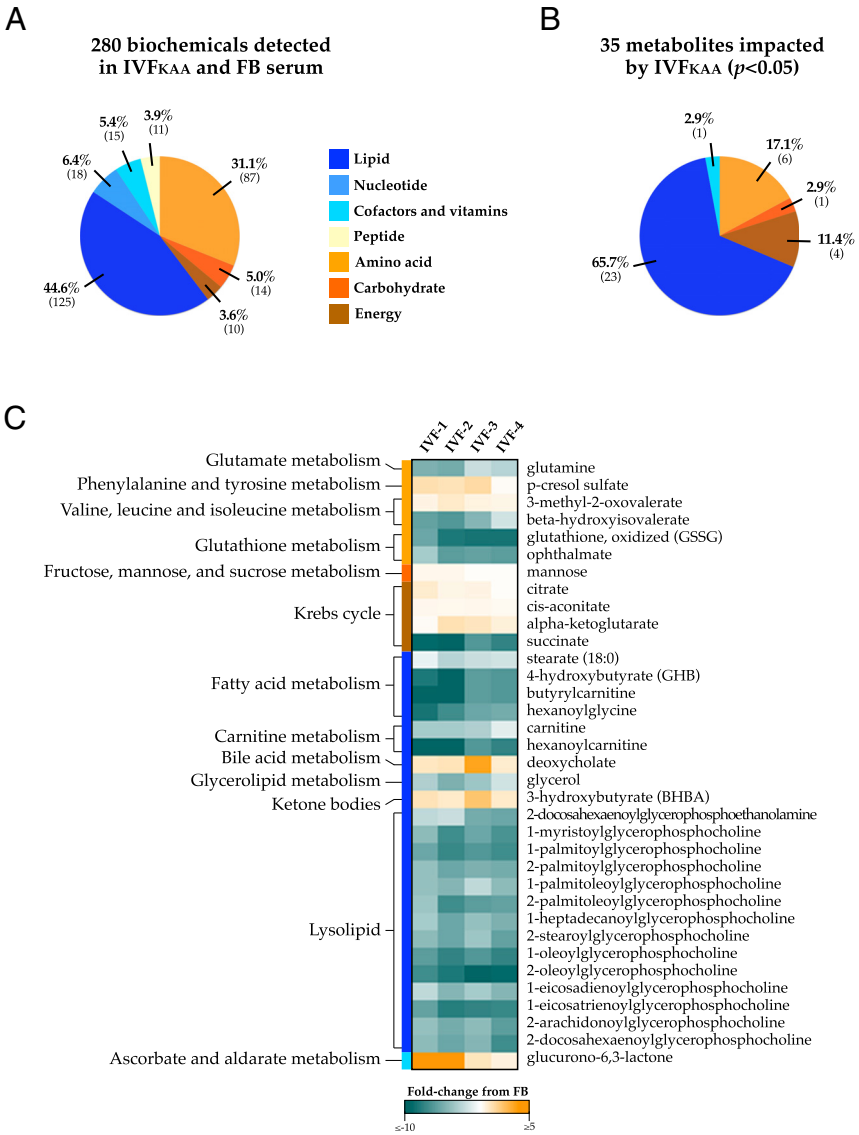

Figure 3. Impact of IVF on the adult serum metabolome. Unbiased metabolic profiling was performed on FB and IVF_{KAA} serum isolated from 29-week-old female mice (Metabolon, Inc.). A, Categorical distribution of the 280 metabolites detected by the analysis, which comprises all major biochemical groups. B, The concentrations of 35 metabolites were significantly altered in IVF mice ($P < .05$) and consisted predominantly of lipid metabolism derivatives. C, Heat map displays the fold-change comparison of biochemical values with their corresponding metabolic pathway measured for each IVF_{KAA} animal relative to control mean values (n = 4 per condition). Notable changes in the IVF_{KAA} serum metabolome include reduced systemic glycerophosphocholines, altered concentrations of trichloroacetic acid (TCA) cycle intermediates, decreased circulating glutamine, and a significant increase in the ketone body 3-hydroxybutyrate (BHBA).

ological observations (Figure 4A). A full list of the significantly misregulated pathways and their associated genes for each tissue is shown in Supplemental Table 3. Interestingly, the degree of concordance in gene expression changes between IVF tissues was minimal (Figure 4B) and not robustly associated with any particular biological theme, indicating that the impact of IVF on the adult transcriptome varies in a tissue-specific manner. To distinguish the most prevalently and significantly altered pathways, P values associated with individual dysregulated pathways were negatively log transformed (here, $-\log(P < .05)$ corresponds to values >1.3) and ranked according to highest combined log score across the 4 tissues. Liver X receptor/retinoid X receptor activation, mitochondrial dysfunction, and type I diabetes mellitus signaling were among the most prominent pathways globally altered following IVF_{KAA} (Figure 4C), demonstrating the prevalence of energy defects in IVF_{KAA} metabolic tissues.

Sustained up-regulation and epigenetic alteration to the *Txnip* locus following IVF_{KAA}

Previous microarray analysis comparing IVF_{WM} and in vivo-generated blastocysts revealed a dramatic up-regulation of *Txnip* (21). Given that Txnip plays an important role in glucose homeostasis and is regulated by epigenetic mechanisms (17, 20), we investigated whether *Txnip* was also misregulated in IVF_{KAA} blastocysts and if this persisted in pancreatic β-cells and insulin-sensitive tissues in the adult.

Analysis by quantitative PCR confirmed that IVF_{KAA} induces a nearly 4-fold increase in *Txnip* transcription (Figure 5A), with a comparable increase in TXNIP protein relative to in vivo-generated blastocysts (Figure 5, B and C). Because subcellular localization of TXNIP is reportedly affected by redox state (36), we performed immunostaining of TXNIP to investigate localization but observed no changes between IVF_{KAA} and FB embryos (Figure 5D). Examination of the chromatin architecture at the *Txnip* promoter in IVF_{KAA} blastocysts revealed an enrichment for the active modification acetylated H4 (H4ac) (37), relative to controls (Figure 5E). Further, there was no change in the heterochromatin marker H4K20me3 between IVF_{KAA} and in vivo-generated blastocysts (Figure 5F) (38). Bisulfite sequencing of the *Txnip* promoter, 5′-untranslated region, and initial coding region detected no changes

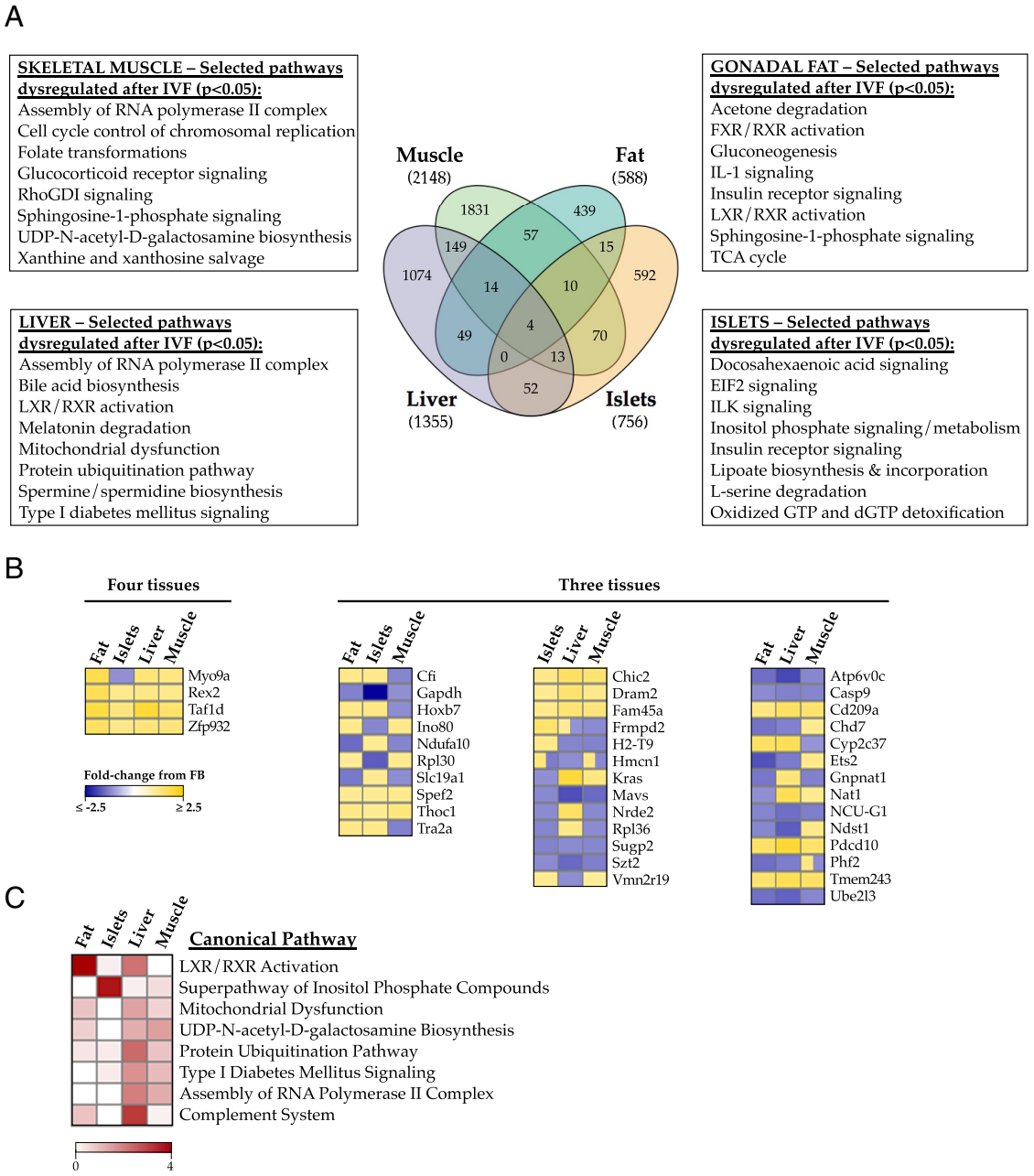

Figure 4. Evidence of metabolic dysfunction across multiple metabolic tissues. Microarray investigation comparing genetic changes in 29-week-old IVF_{KAA} female liver, skeletal muscle, gonadal fat, and pancreatic islets with age- and gender-matched FB controls. A, Venn diagram comparing concordance of gene misexpression after IVF_{KAA} across the 4 tissues, including selected pathways significantly altered compared with controls for each tissue ($P < .05$, based on a 1.2 fold-change cutoff). B, Heat map representation of the genes misexpressed in 3 or more IVF_{KAA} tissues, and their directionality of change. C, Prevalence of dysregulated pathways after IVF_{KAA}. *P* values associated with each misregulated canonical pathway were negatively log transformed and ranked according to highest combined log score across the 4 tissues. The heat map shows the top scoring pathways most commonly disrupted in IVF_{KAA} adult females. LXR, liver X receptor; RXR, retinoid X receptor.

in CpG methylation between conception conditions (Supplemental Figure 7).

We hypothesized that alterations to *Txnip* expression might be maintained into adulthood, and next compared the changes observed in blastocyst *Txnip* regulation with parallel parameters in adult animals. Male IVF_{KAA} mice aged 29 weeks displayed a 2-fold increase in *Txnip* mRNA levels specifically in gonadal fat, but not in pancreas, liver, or muscle (Figure 6A). This corresponded to increased TXNIP protein (Figure 6B), and enrichment of H4ac at the *Txnip* promoter in fat tissue (Figure 6C). In females, *Txnip* expression was similarly increased in fat and additionally muscle after IVF_{KAA}, but not in liver or pancreatic islets (Figure 6A). TXNIP protein was likewise increased in fat and muscle tissues (Figure 6B). As observed in blastocysts, H4ac was enriched at the *Txnip* promoter in IVF_{KAA} fe-

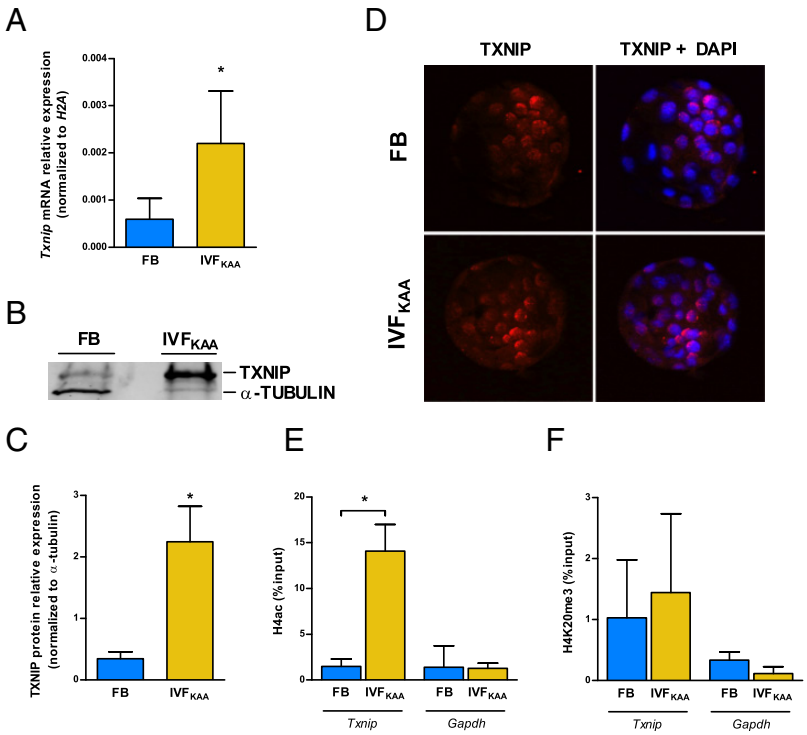

Figure 5. Misregulation of Txnip in IVF_{KAA} blastocysts. A, Txnip mRNA expression relative to H2A in FB (blue) and IVF_{KAA} (yellow) embryos. B, Western blot of TXNIP and β-actin protein with (C) quantification of TXNIP relative expression for both conditions. D, Immunostaining of TXNIP localization (red) with 4′,6-diamidino-2-phenylindole (DAPI) counterstain (blue). E and F, Chromatin immunoprecipitation of (E) H4 acetylation and (F) H4K20me3 enrichment at the Txnip and Gapdh promoters in FB and IVF_{KAA} blastocysts. Error bars depict SD. *, $P < .05$.

male fat, with no change in H4K20me3 (Figure 6, C and D). As a control, chromatin immunoprecipitation for H4ac in female liver did not show enrichment (Figure 6E), indicating a positive correlation between H4ac presence and increased *Txnip* expression. Collectively the data demonstrate a significant effect of IVF_{KAA} on the expression and regulation of the metabolic sensor *Txnip* in blastocysts, with tissue-specific maintenance of these changes in adulthood.

Discussion

Our data demonstrate that IVF and embryo culture, even under optimal conditions, lead to long-term metabolic alterations in a mouse model. This study both confirms the sensitivity of the fertilization and preimplantation stages to environmental influence on postnatal physiology and extends the analysis of embryo culture outcomes into late postnatal life.

It is well known that chemically defined culture conditions can influence blastocyst competence for postimplantation development in both mice (34) and humans (39). Our group and others have previously reported that fertilization and culture of preimplantation embryos in vitro affects rates of blastocyst development, cell number and lineage allocation, gene expression, and placental function in a manner sensitive to both culture medium composition and oxygen tension (3, 13, 15, 21, 40), indicating that modest fluctuations in preimplantation environment can impact embryo metabolism and subsequent viability. Several groups have corroborated the detrimental effects of Whitten's medium as compared with other culture media (13, 41). We therefore designed experiments to test whether a graded degree of preimplantation disturbance would result in escalating alterations to metabolic health in adult mice. We show that culturing embryos using different oxygen tensions and media compositions resulted in sexually dimorphic adult phenotypes. In particular, glucose intolerance follows preimplantation embryo manipulation in a medium- and sex-dependent fashion.

We found that the growth curves of both IVF_{WM} and IVF_{KAA} mice were disturbed, but in different fashions. Male and female IVF_{WM} mice had normal birth weights but their growth failed to keep pace with controls: by 2 weeks of age the IVF_{WM} mice were significantly smaller and remained smaller through puberty and most of adulthood (Figure 1, A and C). On the contrary, only the growth kinetics of female, but not male, IVF_{KAA} mice was altered. IVF_{KAA} females exhibited a "catch-up" growth in which they were significantly smaller at birth, reached the same weight by 1 week of postnatal life, and in adulthood surpassed the body weight of their FB counterparts. Other authors have demonstrated that different preimplantation conditions uniquely affect postnatal growth pattern. For example, Banrezes et al (42) reported that manipulating the redox potential during the pronuclear stage affects postnatal body weight. They demonstrated that exposure of zygotes exclusively to pyruvate as the sole energy source resulted in offspring that were persistently and significantly smaller compared with controls cultured in standard M16 medium, whereas exogenous lactate produced offspring that were smaller prior to weaning but later reached equal weights as the control group. Finally, zygote exposure to cytosolic alkalization significantly increased offspring size after birth. It is well known that low birth weight is a

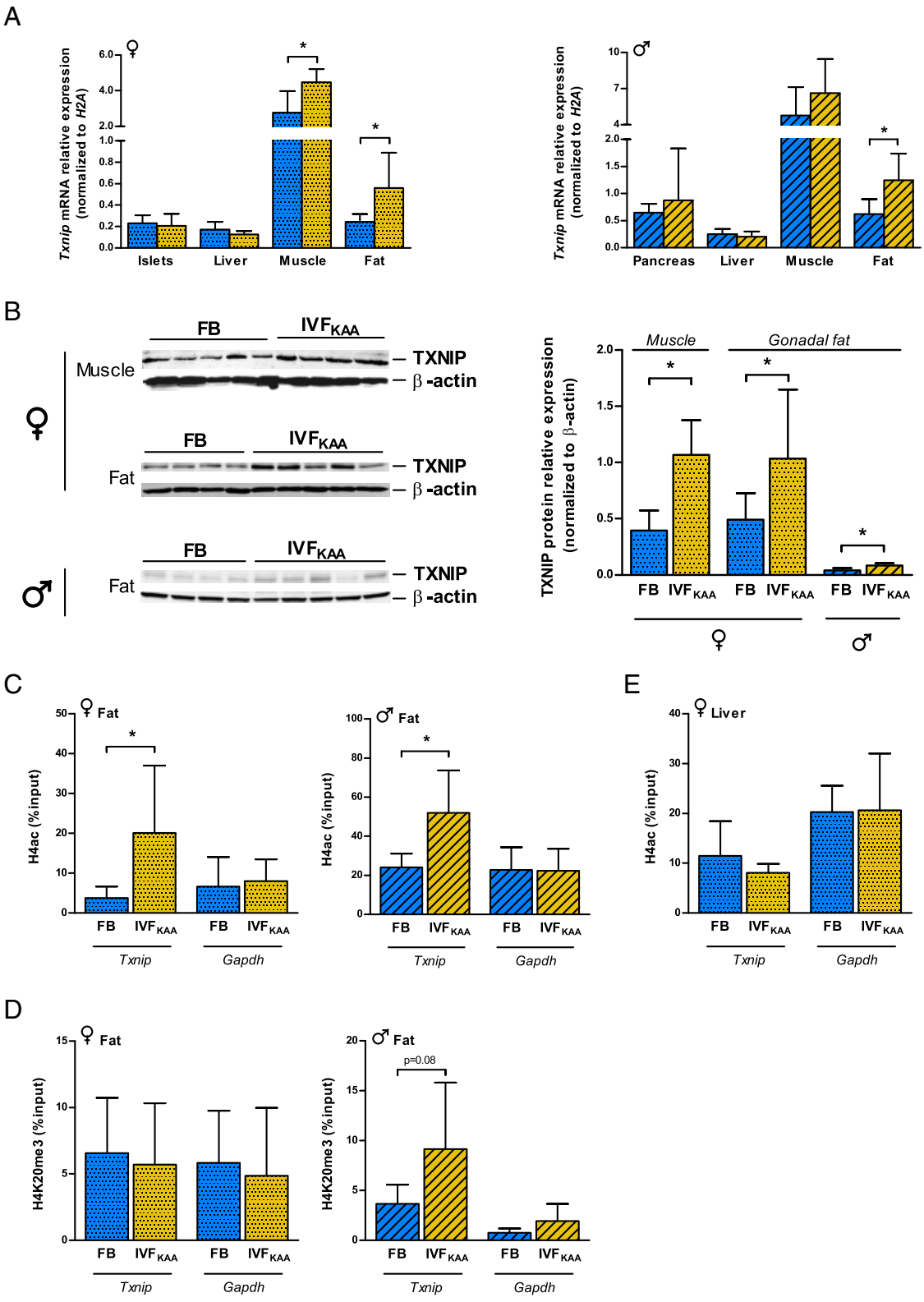

Figure 6. Tissue-specific maintenance of IVF_{KAA}-induced changes to Txnip regulation in 30-week-old mice. A, Txnip mRNA expression relative to H2A in whole pancreas/pancreatic islets, liver, muscle, and fat tissues for female (spotted) and male (hatched) FB (blue) and IVF_{KAA} (yellow) animals. B, Western blot of TXNIP and β-actin expression in female muscle and fat, and male fat tissue, with corresponding quantification of expression. C and D, Chromatin immunoprecipitation at the Txnip and Gapdh promoters in male and female fat tissue for (C) H4ac and (D) H4K20me3 enrichment in FB and IVF_{KAA} adults. E, H4ac enrichment in female liver at Txnip and Gapdh promoters. Error bars depict SD. *, $P <$ .05.

marker of adult cardiovascular and metabolic disease (43), but the authors did not investigate metabolic physiology in these animals.

We additionally observed altered glucose homeostasis following IVF, but the perturbations were significant only in female mice. The conditions under which the IPGTTs were performed were different in the 2 groups. Impaired glucose tolerance was observed in IVF_{WM} mice fasted overnight, a less sensitive protocol for detecting differences in glucose handling than the 6-hour fasting period used for the IVF_{KAA} mice, in which no impairment of glucose tolerance was observed. IVF_{KAA} females, however, did have greater 6-hour fasting glucose levels than controls at 20 and 29 weeks, when these mice had become heavier than their FB counterparts. IVF_{KAA} mice also displayed higher bone mineral density, a feature that is associated with type 2 diabetes mellitus in humans (29). Overall, IVF_{WM} females were more glucose intolerant, with a leaner body mass, than IVF_{KAA} females. Similar phenotypes have been observed in mice generated by somatic cell nuclear transfer (44), or in rodent models of maternal diet-induced obesity (45). Interestingly, in utero caloric restriction is associated with low birth weight, "catch-up" growth, and glucose intolerance specifically in male mice (46). In our study, neither birth weight nor the IVF-associated accelerated growth were linked with glucose intolerance in the ways predicted by previous caloric restriction models. This suggests that although altered glucose homeostasis is a common response to developmental disturbance, the early embryo environment can trigger changes that will affect adult physiology, and the timing at which the stress occurs (ie, preimplantation or in utero) can result in unique phenotypic changes.

Studies of developmental stress also report sexually dimorphic effects following embryo manipulation. A low-protein diet administered exclusively during the preimplantation period was associated with postnatal hypertension in both sexes but resulted in increased weight only in female mice (47). The occurrence of a diabetic or glucose-intolerant state is often sexually dimorphic as well. In the nonobese diabetic mouse model, females develop diabetes more rapidly and with increased severity (48). Interestingly, in the C57Bl/6J strain used in this study, males are generally more glucose intolerant (49). Although the mechanism underlying this sexual dimorphism remains unclear, it may be related to sex-specific regulatory pathways, gonadal hormone differences or hypothalamic-pituitary-adrenal axis control (50, 51). Further, the effects of IVF may influence sexual dimorphism as early as the blastocyst stage, as up to one-third of gene transcripts are differentially expressed between male and female blastocysts (52), which are therefore capable of differentially responding to their environments.

To better define the molecular and metabolic consequences of preimplantation embryo culture, we performed unbiased analyses of both the transcriptomes of adult insulin-sensitive tissues and pancreatic islets using microarray technology, and of serum metabolite composition using mass spectrometry. Because KSOM is the basis for multiple human IVF media used today, and because female IVF_{KAA} mice had a clear phenotype, we focused on the more clinically relevant IVF_{KAA} experimental group. Overall, the gene expression signatures of IVF tissues revealed changes in pathways involved in glucose handling. The most pervasive differences were to genes associated with sterol and fatty acid homeostasis (liver X receptor/retinoid X receptor activation) (53), and glucose metabolism, including inositol phosphate metabolism (ie, PI3K/Akt signaling), type 1 diabetes mellitus signaling, and mitochondrial dysfunction. However, despite the common pathway alterations, the gene misexpression correlating with these networks was highly tissue specific, indicating that adult tissues are uniquely affected by IVF. Although the overlap of gene misexpression between IVF tissues was low, the genes concordantly misexpressed in all 4 IVF tissues were predominantly involved in transcriptional regulation. Moreover, the significance behind the additional pathway changes in IVF mice (UDP-*N*-acetyl-D-galactosamine biosynthesis, assembly of RNA polymerase II complex, complement system) is unclear and will require further investigations.

Importantly, the IVF_{KAA} gene expression profiles were mirrored in serum metabolite signatures, indicating a correlation between the microarray and metabolomics results. Specifically, several of the observed biochemical differences have been similarly noted in metabolomics-based investigations of obesity and diabetes. For example, blocked branched-chain amino acid oxidation and increased ketogenesis is strongly associated with obesity-related insulin resistance in both rats and humans (54); decreased circulating glutamine is a marker of glucose intolerance and insulin resistance in mice and humans (55); and a significant global reduction in serum glycerophospholipid content is correlated with both impaired fasting glucose (56) and diet-induced obesity (57). Overall, the altered concentrations of systemic glycolytic, trichloroacetic acid cycle, and fatty acid derivatives reflect widespread shifts in nutrient usage. Because the metabolomics and microarray analyses were performed using adult tissues, it is unclear which IVF-associated changes were either uncovered or masked by the administration of the high-fat diet, or secondary to in utero and postnatal experiences.

Finally, we focused on the blastocyst, prior to the development of glucose intolerance, to evaluate changes incited by IVF that might contribute directly to the postnatal phenotype. We identified Txnip as a marker of preimplantation stress and demonstrate that the memory of preimplantation disturbance is maintained through *Txnip* misregulation in selected adult tissues (adipose tissue and, to a minor extent, muscle in female mice). Previous studies have highlighted a role for TXNIP in regulating peripheral glucose metabolism (17), and it is now appreciated that *Txnip* misregulation can potentiate diabetes pathogenesis (58, 59). Overall, TXNIP functions as a focal point for integrating cellular nutrition with redox state and helps to regulate mitochondrial function and structural integrity (60). The latter point is particularly relevant because mitochondrial dysfunction (highlighted by our microarray experiments) plays a causative role in the development of insulin resistance (61). It is therefore possible that TXNIP is a key element of the embryo metabolic sensing mechanism and that conception by IVF precipitates metabolic disease through misregulation of *Txnip*. Future studies using genetic models should be designed to assess whether Txnip changes are directly responsible for inducing the observed phenotype. In general, our data suggest that preimplantation stress is associated with specific epigenetic and gene expression changes that persist in adulthood.

It is widely believed that epigenetic changes mediate developmental plasticity and contribute significantly to programming of environmental signals (62). Because epigenetic modifications are extensively remodeled in the preimplantation embryo (63), and because culture conditions can affect chromatin marks (41), we evaluated whether *Txnip* was subjected to epigenetic modification following culture in vitro. Shalev and colleagues (20) previously reported that *Txnip* regulation by glucose is mediated, in part, by H4ac. Similarly, we observed H4ac enrichment at the *Txnip* promoter both in blastocysts and adult adipose tissue, whereas inhibitory chromatin marks and DNA methylation of the *Txnip* promoter were not changed. This suggests that an open chromatin structure was established in the blastocyst following in vitro culture and selectively maintained in the adipose tissue. Greater DNA accessibility could explain the increase in *Txnip* expression.

The reasons for tissue-specific variation in the stability of IVF-induced transcriptional and epigenetic changes throughout in utero and postnatal development are unknown. One explanation is that the molecular changes present in blastocysts following preimplantation disturbance are differentially affected by organogenesis, growth factors, or sexually dimorphic signals occurring during later stages of development. Therefore, cell physiology and metabolism within each developing tissue may be altered in accordance with new, tissue-specific developmental cues. Further, our data suggest that adipose tissue may be a locus where preimplantation stress-induced reprogramming is maintained. This is particularly relevant because fat is now regarded as a primary driver of systemic metabolic dysfunction (64).

A few factors should be acknowledged while analyzing this study. We did not use an in vivo control group following natural mating because we wanted to specifically test the impact of IVF and embryo culture, while removing variables such as superovulation and the embryo transfer procedure. The former strategy results in significantly different litter sizes (preliminary studies; data not shown). Studies on neonatal programming clearly show distinct growth patterns associated with substantial differences in litter size (12). The use of the FB cohort allowed us to generate recipients with equivalent, although not identical, litter sizes.

Separately, the administration of a high-fat diet makes the interpretation of the results more complex. However, both the experimental and control groups received and were equally affected by the diet. Because the increase in weight and fat deposition in IVF_{KAA} female mice preceded the change in diet, this suggests a nutrition-independent effect of IVF on postnatal growth and body composition.

Finally, due to the broad differences in composition of the culture media used in the IVF groups, we cannot link a particular preimplantation culture condition to a specific adult phenotype. Future studies should be designed to assess how the adult phenotype is affected by changing a single culture parameter (eg, only oxygen tension, carbohydrate, or amino acid energy substrate) while maintaining all other components constant.

In conclusion, our data support the view that preimplantation development is an environmentally sensitive period and that preimplantation embryos are vulnerable to environmental disturbances, which can permanently program growth trajectory and energy homeostasis in the developing and adult individual through transcriptional, epigenetic, and metabolic mechanisms. Although the results found in this study might not have direct implication to humans given the species-specific differences in development, these data underscore the importance of continued follow-up of IVF-conceived offspring beyond early postnatal life.

Acknowledgments

We thank Dr Richard Weiner for his thoughtful discussion and critical reading of this manuscript. We also thank Charles

Wilkinson for graciously performing the corticosterone RIA and Kirk Pappan at Metabolon, Inc, for his help processing the metabolomics data.

Address all correspondence and requests for reprints to: Paolo Rinaudo, MD, PhD, Obstetrics, Gynecology, and Reproductive Sciences, University of California San Francisco, San Francisco, CA 94115. E-mail: rinaudop@obgyn.ucsf.edu.

This work was supported by a National Institute of Child Health and Human Development (NICHD) grant (RO1:HD 062803–01A1) and American Diabetes Association grant (to P.F.R.). S.K.F. was supported by a National Institute of Health (NIH) training fellowship (5T32DK007418–32). R.K.S. was supported by the California Institute for Regenerative Medicine (TB1–01194).

Disclosure Summary: The authors have nothing to disclose.

References

1. **Wadhwa PD, Buss C, Entringer S, Swanson JM.** Developmental origins of health and disease: brief history of the approach and current focus on epigenetic mechanisms. *Semin Reprod Med*. 2009;27:358–368.
2. **Kwong WY, Wild AE, Roberts P, Willis AC, Fleming TP.** Maternal undernutrition during the preimplantation period of rat development causes blastocyst abnormalities and programming of postnatal hypertension. *Development*. 2000;127:4195–4202.
3. **Ecker DJ, Stein P, Xu Z, et al.** Long-term effects of culture of preimplantation mouse embryos on behavior. *Proc Natl Acad Sci USA*. 2004;101:1595–1600.
4. **Leese HJ.** Metabolism of the preimplantation embryo: 40 years on. *Reproduction*. 2012;143:417–427.
5. **Feuer SK, F. RP.** Preimplantation stress and development. *Birth Defects Res C*. 2012;96:299–314.
6. **ICMART 2012 International Committee.** Monitoring assisted reproductive technology (ICMART) world report: preliminary 2008 data. ESHRE, July 2, 2012. www.eshre.eu/eshre/English/press-room/press-releases/press-releases-2012/5-million-babies/page.aspx/1606.
7. **Feuer SK, Camarano L, Rinaudo PF.** ART and health: clinical outcomes and insights on molecular mechanisms from rodent studies. *Mol Hum Reprod*. 2013;19:189–204.
8. **Ceelen M, van Weissenbruch MM, Vermeiden JP, van Leeuwen FE, Delemarre-van de Waal HA.** Cardiometabolic differences in children born after in vitro fertilization: follow-up study. *J Clin Endocrinol Metab*. 2008;93:1682–1688.
9. **Ceelen M, van Weissenbruch MM, Prein J, et al.** Growth during infancy and early childhood in relation to blood pressure and body fat measures at age 8–18 years of IVF children and spontaneously conceived controls born to subfertile parents. *Hum Reprod*. 2009;24:2788–2795.
10. **Miles HL, Hofman PL, Peek J, et al.** In vitro fertilization improves childhood growth and metabolism. *J Clin Endocrinol Metab*. 2007;92:3441–3445.
11. **Rinaudo P, Schultz RM.** Effects of embryo culture on global pattern of gene expression in preimplantation mouse embryos. *Reproduction*. 2004;128:301–311.
12. **Aubert R, Suquet JP, Lemonnier D.** Long-term morphological and metabolic effects of early under- and over-nutrition in mice. *J Nutr*. 1980;110:649–661.
13. **Rinaudo PF, Giritharan G, Talbi S, Dobson AT, Schultz RM.** Effects of oxygen tension on gene expression in preimplantation mouse embryos. *Fertil Steril*. 2006;86(Suppl 4)1252–1265.
14. **Delle Piane L, Lin W, Liu X, et al.** Effect of the method of conception and embryo transfer procedure on mid-gestation placenta and fetal development in an IVF mouse model. *Hum Reprod*. 2010;25:2039–2046.
15. **Bloise E, Lin W, Liu X, et al.** Impaired placental nutrient transport in mice generated by in vitro fertilization. *Endocrinology*. 2012;153:3457–3467.
16. **Rivera RM, Stein P, Weaver JR, Mager J, Schultz RM, Bartolomei MS.** Manipulations of mouse embryos prior to implantation result in aberrant expression of imprinted genes on day 9.5 of development. *Hum Mol Genet*. 2008;17:1–14.
17. **Parikh H, Carlsson E, Chutkow WA, et al.** TXNIP regulates peripheral glucose metabolism in humans. *PLoS Med*. 2007;4:e158.
18. **Schulze PC, Yoshioka J, Takahashi T, He Z, King GL, Lee RT.** Hyperglycemia promotes oxidative stress through inhibition of thioredoxin function by thioredoxin-interacting protein. *J Biol Chem*. 2004;279:30369–30374.
19. **Chen J, Saxena G, Mungrue IN, Lusis AJ, Shalev A.** Thioredoxin-interacting protein: a critical link between glucose toxicity and β-cell apoptosis. *Diabetes*. 2008;57:938–944.
20. **Cha-Molstad H, Saxena G, Chen J, Shalev A.** Glucose-stimulated expression of Txnip is mediated by carbohydrate response element-binding protein, p300, and histone H4 acetylation in pancreatic β cells. *J Biol Chem*. 2009;284:16898–16905.
21. **Giritharan G, Talbi S, Donjacour A, Di Sebastiano F, Dobson AT, Rinaudo PF.** Effect of in vitro fertilization on gene expression and development of mouse preimplantation embryos. *Reproduction*. 2007;134:63–72.
22. **Epstein HT.** The effect of litter size on weight gain in mice. *J Nutr*. 1978;108:120–123.
23. **Nyengaard JR.** Stereologic methods and their application in kidney research. *J Am Soc Nephrol*. 1999;10:1100–1123.
24. **Larsen MO, Rolin B, Sturis J, et al** Measurements of insulin responses as predictive markers of pancreatic β-cell mass in normal and β-cell-reduced lean and obese Göttingen minipigs in vivo. *Am J Physiol Endocrinol Metab*. 2006;290:E670–E677.
25. **Heikkinen S, Argmann CA, Champy MF, Auwerx J.** Evaluation of glucose homeostasis. *Curr Protoc Mol Biol Chapter*. 2007;29:Unit 29B 23.
26. **Andrikopoulos S, Blair AR, Deluca N, Fam BC, Proietto J.** Evaluating the glucose tolerance test in mice. *Am J Physiol Endocrinol Metab*. 2008;295:E1323–E1332.
27. **Wilkinson CW, Raff H.** Comparative evaluation of a new immunoradiometric assay for corticotropin. *Clin Chem Lab Med*. 2006;44:669–671.
28. **O'Dowd JF.** The isolation and purification of rodent pancreatic islets of Langerhans. *Methods Mol Biol*. 2009;560:37–42.
29. **Giritharan G, Delle Piane L, Donjacour A, et al.** In vitro culture of mouse embryos reduces differential gene expression between inner cell mass and trophectoderm. *Reprod Sci*. 2012;19:243–252.
30. **Evans AM, DeHaven CD, Barrett T, Mitchell M, Milgram E.** Integrated, nontargeted ultrahigh performance liquid chromatography/electrospray ionization tandem mass spectrometry platform for the identification and relative quantification of the small-molecule complement of biological systems. *Anal Chem*. 2009;81:6656–6667.
31. **Dahl JA, Collas P.** A rapid micro chromatin immunoprecipitation assay (microChIP). *Nat Protoc*. 2008;3:1032–1045.
32. **Dean A, Sharpe RM.** Anogenital distance or digit length ratio as measures of fetal androgen exposure: relationship to male reproductive development and its disorders. *J Clin Endocrinol Metab*. 2013;98:2230–2238.
33. **Eriksson JG, Forsen TJ, Osmond C, Barker DJ.** Pathways of infant and childhood growth that lead to type 2 diabetes. *Diabetes Care*. 2003;26:3006–3010.
34. **Schwarzer C, Esteves TC, Araúzo-Bravo MJ, et al.** ART culture conditions change the probability of mouse embryo gestation

through defined cellular and molecular responses. *Hum Reprod*. 2012;27:2627–2640.
35. **Li CC, Young PE, Maloney CA, et al.** Maternal obesity and diabetes induces latent metabolic defects and widespread epigenetic changes in isogenic mice. *Epigenetics*. 2013;8:602–611.
36. **Saxena G, Chen J, Shalev A.** Intracellular shuttling and mitochondrial function of thioredoxin-interacting protein. *J Biol Chem*. 2010;285:3997–4005.
37. **Clayton AL, Hazzalin CA, Mahadevan LC.** Enhanced histone acetylation and transcription: a dynamic perspective. *Mol Cell*. 2006; 23:289–296.
38. **Schotta G, Lachner M, Sarma K, et al.** A silencing pathway to induce H3–K9 and H4–K20 trimethylation at constitutive heterochromatin. *Genes Dev*. 2004;18:1251–1262.
39. **Dumoulin JC, Land JA, Van Montfoort AP, et al.** Effect of in vitro culture of human embryos on birthweight of newborns. *Hum Reprod*. 2010;25:605–612.
40. **Fernández-Gonzalez R, Moreira P, Bilbao A, et al.** Long-term effect of in vitro culture of mouse embryos with serum on mRNA expression of imprinting genes, development, and behavior. *Proc Natl Acad Sci USA*. 2004;101:5880–5885.
41. **Doherty AS, Mann MR, Tremblay KD, Bartolomei MS, Schultz RM.** Differential effects of culture on imprinted H19 expression in the preimplantation mouse embryo. *Biol Reprod*. 2000;62:1526–1535.
42. **Banrezes B, Sainte-Beuve T, Canon E, Schultz RM, Cancela J, Ozil JP.** Adult body weight is programmed by a redox-regulated and energy-dependent process during the pronuclear stage in mouse. *PLoS One*. 2011;6:e29388.
43. **Barker DJ.** *Mothers, Babies and Health in Later Life*. 2nd ed. Glasgow, Scotland: Churchill Livingston; 1998.
44. **Scott KA, Yamazaki Y, Yamamoto M, et al.** Glucose parameters are altered in mouse offspring produced by assisted reproductive technologies and somatic cell nuclear transfer. *Biol Reprod*. 2010;83: 220–227.
45. **Jungheim ES, Schoeller EL, Marquard KL, Louden ED, Schaffer JE, Moley KH.** Diet-induced obesity model: abnormal oocytes and persistent growth abnormalities in the offspring. *Endocrinology*. 2010; 151:4039–4046.
46. **Jimenez-Chillaron JC, Hernandez-Valencia M, Lightner A, et al.** Reductions in caloric intake and early postnatal growth prevent glucose intolerance and obesity associated with low birthweight. *Diabetologia*. 2006;49:1974–1984.
47. **Watkins AJ, Ursell E, Panton R, et al.** Adaptive responses by mouse early embryos to maternal diet protect fetal growth but predispose to adult onset disease. *Biol Reprod*. 2008;78:299–306.
48. **Makino S, Kunimoto K, Muraoka Y, Mizushima Y, Katagiri K, Tochino Y.** Breeding of a non-obese, diabetic strain of mice. *Jikken Dobutsu*. 1980;29:1–13.
49. **Toye AA, Lippiat JD, Proks P, et al.** A genetic and physiological study of impaired glucose homeostasis control in C57BL/6J mice. *Diabetologia*. 2005;48:675–686.
50. **Gabory A, Roseboom TJ, Moore T, Moore LG, Junien C.** Placental contribution to the origins of sexual dimorphism in health and diseases: sex chromosomes and epigenetics. *Biol Sex Differ*. 2013;4:5.
51. **Gutierrez-Adan A, Perez-Crespo M, Fernandez-Gonzalez R, et al.** Developmental consequences of sexual dimorphism during pre-implantation embryonic development. *Reprod Domest Anim*. 2006; 41(Suppl 2):54–62.
52. **Fernández-Gonzalez R, de Dios Hourcade J, López-Vidriero I, Benguria A, De Fonseca FR, Gutiérrez-Adan A.** Analysis of gene transcription alterations at the blastocyst stage related to the long-term consequences of in vitro culture in mice. *Reproduction*. 2009;137: 271–283.
53. **Kalaany NY, Gauthier KC, Zavacki AM, et al.** LXRs regulate the balance between fat storage and oxidation. *Cell Metab*. 2005;1: 231–244.
54. **Newgard CB, An J, Bain JR, et al.** A branched-chain amino acid-related metabolic signature that differentiates obese and lean humans and contributes to insulin resistance. *Cell Metab*. 2009;9:311–326.
55. **Cheng S, Rhee EP, Larson MG, et al.** Metabolite profiling identifies pathways associated with metabolic risk in humans. *Circulation*. 2012;125:2222–2231.
56. **Xu F, Tavintharan S, Sum CF, Woon K, Lim SC, Ong CN.** Metabolic signature shift in type 2 diabetes mellitus revealed by mass spectrometry-based metabolomics. *J Clin Endocrinol Metab*. 2013;98: E1060–E1065.
57. **Kim HJ, Kim JH, Noh S, Hur HJ, Sung MJ, Hwang JT, Park JH, Yang HJ, Kim MS, Kwon DY, Yoon SH.** Metabolomic analysis of livers and serum from high-fat diet induced obese mice. *J Proteome Res*. 2011;10:722–731.
58. **Shalev A.** Lack of TXNIP protects β-cells against glucotoxicity. *Biochem Soc Trans*. 2008;36:963–965.
59. **Wu N, Zheng B, Shaywitz A, et al.** AMPK-dependent degradation of TXNIP upon energy stress leads to enhanced glucose uptake via GLUT1. *Mol Cell*. 2013;49:1167–1175.
60. **Yoshioka J, Chutkow WA, Lee S, et al.** Deletion of thioredoxin-interacting protein in mice impairs mitochondrial function but protects the myocardium from ischemia-reperfusion injury. *J Clin Invest*. 2012;122:267–279.
61. **Morino K, Petersen KF, Shulman GI.** Molecular mechanisms of insulin resistance in humans and their potential links with mitochondrial dysfunction. *Diabetes*. 2006;55(Suppl 2):S9–S15.
62. **Gluckman PD, Hanson MA, Low FM.** The role of developmental plasticity and epigenetics in human health. *Birth Defects Res C Embryo Today*. 2011;93:12–18.
63. **Reik W.** Stability and flexibility of epigenetic gene regulation in mammalian development. *Nature*. 2007;447:425–432.
64. **Muoio DM, Newgard CB.** Obesity-related derangements in metabolic regulation. *Annu Rev Biochem*. 2006;75:367–401.